



RESEARCH ARTICLE | JULY 25 2023

Strain-tuned optical conductivity of monolayer PbBi FREE

Bui D. Hoi  



Journal of Applied Physics 134, 045104 (2023)

<https://doi.org/10.1063/5.0154826>



CrossMark

500 kHz or 8.5 GHz?
And all the ranges in between.

Lock-in Amplifiers for your periodic signal measurements



Find out more



Strain-tuned optical conductivity of monolayer PbBi

Cite as: J. Appl. Phys. 134, 045104 (2023); doi: 10.1063/5.0154826

Submitted: 16 April 2023 · Accepted: 10 July 2023 ·

Published Online: 25 July 2023



Bui D. Hoi^{a)}

AFFILIATIONS

Faculty of Physics, University of Education, Hue University, Hue 530000, Vietnam

^{a)}Author to whom correspondence should be addressed: buidinhhoi@hueuni.edu.vn

ABSTRACT

In this paper, we investigate the optical response of the PbBi single-layer by developing a strain-induced Kane–Mele model from Peierls substitution and by employing the Kubo formula at low temperatures. We address three different regimes of uniform and non-uniform classes created by tuning the strength of the strain. From a detailed analysis of the electronic band structure, we find that the Rashba spin splitting gap is destroyed with strain, while the bulk gap slightly changes. We also find that interband optical transitions exhibit a blueshift spectrum with strain. Interestingly, all these findings are independent of the regime and class of strain. However, our simulations show that only the non-uniform class of strain leads to anisotropic optical conductivity. These results enhance optoelectronic applications of low-dimensional materials.

Published under an exclusive license by AIP Publishing. <https://doi.org/10.1063/5.0154826>

I. INTRODUCTION

In contrast to the first two-dimensional (2D) topological insulator—graphene—with limited proposals for practical applications,^{1–3} quantum spin Hall insulators (QSHIs) provide important applications^{4,5} due to the presence of fully spin-polarized helical edge modes and intrinsic spin–orbit coupling (SOC).^{6–10} There also exist compounds of heavy elements such as Bi, Pb, and W with extrinsic Rashba SOCs^{11–15} that have provided interesting chiral spin textures^{16–19} for spintronic applications.

It has been well known that there are various factors such as bias voltage,^{6–8} electron–electron interaction,^{20–26} and magnetic field^{27–31} to tune the properties of QSHIs. Applying strain is also a well-known technique to control the electronic properties of materials, which, in turn, affects all other physical features of the system.^{32–34} Sun *et al.*³⁵ showed that strain can switch topological phase transition between a QAHI and a 2D topological crystalline insulator in an intrinsic ferromagnetic NpSb monolayer. Zhang *et al.*³⁶ predicted that a unique 2D topological insulator with a sizable bulk gap can be formed by a suitable strain modulation of honeycomb arsenene. Ma *et al.*³⁷ showed that an isolated GeCH₃ layer can be a QSHI under a reasonable strain. Huang *et al.*³⁸ found that the exchange energy and nontrivial bandgap in ferromagnetic transition metal halides can be modulated by applying in-plane strain. Since these effects mainly appear in the electronic

band structure of materials, one immediate application can be extracted from optical features.

In addition to Hall insulators, strain engineering is believed to be an effective and suitable way to tune the electro-optical properties of novel 2D monolayer materials which have exceptional mechanical flexibility and strength. It has been shown in MoS₂ and WS₂ monolayers that with increasing strain, the exciton binding energy is nearly unchanged, while optical gap is reduced significantly.³⁹ The redshift or blueshift in the photoluminescence and absorption spectra has been observed in some 2D transition metal dichalcogenides when applying a tensile or compressive strain.^{40,41} In addition, many interesting nonlinear optical properties, including second harmonic generation and third harmonic generation, can be observed under strain in 2D materials with broken inversion symmetry such as transition metal dichalcogenides monolayers.^{42,43} Under the strain, the lattice of a 2D material is distorted and the lattice symmetry is broken, thereby the optical conductivity of the material is altered.⁴³ Also, the direction of applied strain can be expressed by polarization-resolved second harmonic generation.⁴³ Practically, the strain-dependent optical properties are the basis for applications in flexible optoelectronic devices based on 2D materials, such as flexible photodetectors⁴³ and phototransistors.⁴¹

In 2016, monolayer buckled PbBi was theoretically reported by Mera Acosta *et al.*⁴⁴ as a proper QSHI candidate for spintronic

03 August 2023 13:09:43

applications due to its unconventional spin texture and Rashba-like SOC. The applicability of this material stems from the time-reversal symmetry which protects both the edge and bulk states, which, in turn, means that less energy can be lost by this compound when coupling to the environment. However, to the best of our knowledge, the strain effect on the optical properties of PbBiI has not been addressed so far. In this structure, the stacking between Pb–Bi bonds and I atoms is weak^{44–50} and the effective strain can be considered in the plane of the system. This means that the contribution of Pb–I dimers in modulations via strain is negligible.

Given this background, in this work, we apply an in-plane strain (both compressive and tensile) in two uniform and non-uniform classes to see how strain-tuned hopping energies in the electronic band structure of monolayer PbBiI affect its optical conductivity. In contrast to e.g., silicene with the same buckled structure, unconventional spin texture in PbBiI results in a forbidden backscattering mechanism of electrons. So, engineering of optical performance in monolayer PbBiI is highly desirable for practical applications such that electrons in PbBiI have a specific transport channel rather than scattered ones in other similar systems. In doing so, we employ the Kane–Mele model and Kubo formula. The study of optical transitions in this material provides tunable optoelectronic devices. For instance, the blueshift optical spectrum is useful for solar cell applications such that the system can absorb short light wavelengths of sunrise or sunset in addition to the daytime absorptions.

The organization of the paper is as follows: In Sec. II, we present the Kane–Mele Hamiltonian of pristine and strained monolayer PbBiI. In Sec. III, we present the Kubo formula for optical conductivity. In Sec. IV, we turn to the numerical results of electronic band structure and optical conductivity. Finally, we end the paper with a brief overview of our findings in Sec. V.

II. HAMILTONIAN MODEL

Monolayer PbBiI has a honeycomb lattice with the bond lengths d and h along the z -direction, as shown in Fig. 1. It has been well established by Acosta *et al.*⁴⁴ that Bi orbitals mainly build the effective Hamiltonian of the system. Thus, one needs to work with the SOC basis $|J, j_z\rangle$ of Bi atoms with total angular momentum J and spin direction j_z .^{48–50} As mentioned in Sec. I, the $|(Pb-I)_{j,j_z}\rangle$ contribution is negligible. For the matrix elements of the Hamiltonian, let us use $h_{ij} = \sum_{p=1}^6 t_{ap}^{ij} e^{i\vec{k}_p \cdot \vec{a}_p}$ (including momentum \vec{k}_p with respect to the nearest neighbor at the distance

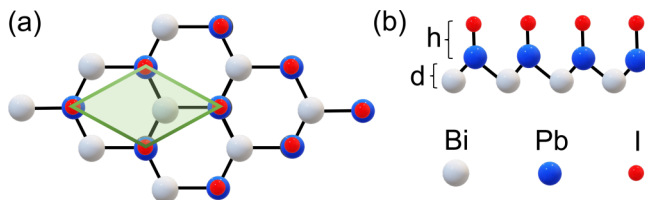


FIG. 1. (a) Top and (b) side sketch of monolayer PbBiI with $h \simeq 1.35 \text{ \AA}$ and $d \simeq 1.3 \text{ \AA}$. The shaded part shows the unit cell of the structure.

\vec{a}_p) for six next nearest neighbor hopping terms $t_{ap}^{ij} = \langle \vec{a}_{p'} | \text{Bi}_{j',j'_z} | \mathcal{H} | \vec{a}_p, \text{Bi}_{j,j_z} \rangle$ with $i = (J, j_z)$ and $j = (J', j'_z)$. With the help of the geometric structure of monolayer PbBiI, we find the following Hamiltonian matrix elements for basis $1 = |1/2, 1/2\rangle$, $2 = |1/2, -1/2\rangle$, $3 = |3/2, 1/2\rangle$, and $4 = |3/2, -1/2\rangle$.^{44,51}

$$h_{11} = \epsilon_{J=1/2} + 2\Re[t^{11}] \sum_{p=1}^3 \cos(k_p) - 2\Im[t^{11}] \sum_{p=1}^3 \sin(k_p), \quad (1a)$$

$$h_{12} = -2i t^{12} [\sin(k_1) + e^{-2i\pi/3} \sin(k_2) + e^{2i\pi/3} \sin(k_3)], \quad (1b)$$

$$h_{13} = 2i \Im[t^{13}] \sum_{p=1}^3 \cos(k_p) + 2i \Re[t^{13}] \sum_{p=1}^3 \sin(k_p), \quad (1c)$$

$$h_{14} = 2\Re[t^{14}] [\cos(k_1) + e^{-2i\pi/3} \cos(k_2) + e^{-4i\pi/3} \cos(k_3)] + 2\Im[t^{14}] [\sin(k_1) + e^{-2i\pi/3} \sin(k_2) + e^{-4i\pi/3} \sin(k_3)], \quad (1d)$$

$$h_{22} = \epsilon_{J=1/2} + 2\Re[t^{11}] \sum_{p=1}^3 \cos(k_p) + 2\Im[t^{11}] \sum_{p=1}^3 \sin(k_p), \quad (1e)$$

$$h_{24} = -2i \Im[t^{13}] \sum_{p=1}^3 \cos(k_p) + 2i \Re[t^{13}] \sum_{p=1}^3 \sin(k_p), \quad (1f)$$

$$h_{33} = \epsilon_{J=3/2} + 2\Re[t^{33}] \sum_{p=1}^3 \cos(k_p) - 2\Im[t^{33}] \sum_{p=1}^3 \sin(k_p), \quad (1g)$$

$$h_{34} = -2i t^{34} [\sin(k_1) + e^{-2i\pi/3} \sin(k_2) + e^{2i\pi/3} \sin(k_3)], \quad (1h)$$

$$h_{44} = \epsilon_{J=3/2} + 2\Re[t^{33}] \sum_{p=1}^3 \cos(k_p) + 2\Im[t^{33}] \sum_{p=1}^3 \sin(k_p), \quad (1i)$$

where $\epsilon_J = t_0^{ii} + 6\Re[t^{ii}]$, $h_{21} = h_{12}^*$, $h_{23} = -h_{14}^*$, $h_{31} = h_{13}^*$, $h_{32} = h_{23}^*$, $h_{41} = h_{14}^*$, $h_{42} = h_{24}^*$, and $h_{43} = h_{34}^*$. For simplicity, without losing the accuracy of calculations, we simplify these expressions by taking the low-energy limit around small momentum up to the second order in k (a single momentum left after expansion up to the second order in all k_p s). Let us use the notations $\zeta_J = 3a^2 \Re[t^{ii}]/3$ ($a \simeq 4.3 \text{ \AA}$ being the lattice constant), $\alpha_{R,1/2} \simeq 3at^{12}$, and $\gamma = 3\Im[t^{14}]$. By neglecting warping effects, we

set $t^{34} \approx 0$. Hence, we find

$$\mathcal{H}_{\vec{k}} = \begin{pmatrix} -\varepsilon_{1/2} & 0 & 0 & 0 \\ 0 & -\varepsilon_{1/2} & 0 & 0 \\ 0 & 0 & +\varepsilon_{3/2} & 0 \\ 0 & 0 & 0 & +\varepsilon_{3/2} \end{pmatrix} + \begin{pmatrix} \zeta_{1/2}k^2 & i\alpha_{R,1/2}k_- & 0 & \gamma k_- \\ -i\alpha_{R,1/2}k_+ & \zeta_{1/2}k^2 & \gamma k_+ & 0 \\ 0 & \gamma k_- & -\zeta_{3/2}k^2 & 0 \\ \gamma k_+ & 0 & 0 & -\zeta_{3/2}k^2 \end{pmatrix}, \quad (2)$$

where $\varepsilon_{1/2} = 0.1685$ eV, $\varepsilon_{3/2} = 0.1575$ eV, $\zeta_{1/2} = 0.0081870.008187$ eV/Å², $\zeta_{3/2} = 0.0380680.038068$ eV/Å², $\alpha_{R,1/2} = 3.0919$ eV/Å, and $\gamma = -3.5853$ eV/Å. In the above Hamiltonian, we use $k_{\pm} = k_x \pm ik_y$ and $k^2 = k_x^2 + k_y^2$.

The energy dispersion has the form

$$\mathcal{E}_{\vec{k},\nu}^{\tau} = \frac{1}{2} \left[v\alpha_{R,1/2}k + \varepsilon + \zeta k^2 + \tau \mathcal{G}_{\nu}(\vec{k}) \right], \quad (3a)$$

$$\mathcal{G}_{\nu}(\vec{k}) = \sqrt{Ck^2 + (\tilde{\varepsilon} - \tilde{\zeta}k^2)(-2v\alpha_{R,1/2}k + \tilde{\varepsilon} - \tilde{\zeta}k^2)}. \quad (3b)$$

Here, $\varepsilon = \varepsilon_{3/2} - \varepsilon_{1/2}$, $\zeta = \zeta_{1/2} - \zeta_{3/2}$, $\tilde{\varepsilon} = \varepsilon_{3/2} + \varepsilon_{1/2}$, $\tilde{\zeta} = \zeta_{1/2} + \zeta_{3/2}$, and $C = 4\gamma^2 + \alpha_{R,1/2}^2$. Also, $\nu = \pm 1$ shows the total angular momentum $J = 3/2$ ($\nu = +1$) and $J = 1/2$ ($\nu = -1$), while $\tau = \pm 1$ shows the spin direction $j_z = -1/2$ ($\tau = +1$) and $j_z = +1/2$ ($\tau = -1$).

Now, we turn to the strained monolayer PbBiI. Although there are various ways to include strain in the pristine Hamiltonian, an alternative way is based on a direct expansion of the hopping parameters t^{ij} such that $t e^{i\vec{k}_p \cdot \vec{a}_p} \rightarrow t e^{i\vec{k}_p \cdot \vec{a}_p} e^{-i\vec{e}\vec{A} \cdot \vec{a}_p}$ ($\hbar = 1$), where the extra phase factor is due to gauge mechanical vector potential $\vec{A} = (A_x, A_y)$. In this mechanism, the strain due to weak lattice deformations leads to a linear shifted/tilted momentum space and the contribution of strains can be expressed by a shift in the momentum $\vec{k} \mapsto \vec{k} + \vec{A}$, where \vec{A} is the characteristic parameter for strain effects in our model.⁵² It mainly originates from a gauge mechanical vector potential similar to the Peierls substitution. It should be noted that there is an inversion symmetry between compressive and tensile strains due to the presence of the Rashba term.

III. OPTICAL CONDUCTIVITY

To calculate the optical conductivity of monolayer PbBiI in the absence and presence of strain, we use the linear response theory in terms of the current-current correlation function⁵³⁻⁵⁵

$$\mathcal{J}_{\alpha\beta,\nu\nu'}^{m'}(\vec{k}) = \langle \vec{k}; \nu, \eta | j_{\alpha} | \vec{k}; \nu', \eta' \rangle \langle \vec{k}; \nu', \eta' | j_{\beta} | \vec{k}; \nu, \eta \rangle, \quad (4)$$

where $\{\nu, \eta\}$ and $\{\nu', \eta'\}$ stand for the bands and $\{\alpha, \beta\} = \{x, y\}$ refers to different directions for currents. The tensor quantity $\mathcal{J}_{\alpha\beta,\nu\nu'}^{m'}(\vec{k})$, dipole elements, determines the correlation between currents along different directions, which can be given by the

components of the current operator $j_{\alpha} = e\partial\mathcal{H}_{\vec{k}}/\partial k_{\alpha}$,

$$j_x = e \begin{pmatrix} 2\zeta_{1/2}k_x & i\alpha_{R,1/2} & 0 & \gamma \\ -i\alpha_{R,1/2} & 2\zeta_{1/2}k_x & \gamma & 0 \\ 0 & \gamma & -2\zeta_{3/2}k_x & 0 \\ \gamma & 0 & 0 & -2\zeta_{3/2}k_x \end{pmatrix}, \quad (5a)$$

$$j_y = e \begin{pmatrix} 2\zeta_{1/2}k_y & \alpha_{R,1/2} & 0 & -i\gamma \\ \alpha_{R,1/2} & 2\zeta_{1/2}k_y & i\gamma & 0 \\ 0 & -i\gamma & -2\zeta_{3/2}k_y & 0 \\ i\gamma & 0 & 0 & -2\zeta_{3/2}k_y \end{pmatrix}. \quad (5b)$$

It is easy to find the eigenstates in the pristine state,

$$|\vec{k}; \nu, \eta\rangle = |J, j_z\rangle = \frac{e^{i\nu\pi/2}}{\sqrt{N_i}} \begin{pmatrix} e^{i\nu\pi/2} \mathcal{D}_{\nu}^{\eta} \\ \mathcal{D}_{\nu+2}^{\eta} \\ \mathcal{D}_{\nu}^{\eta+2} \\ e^{i\nu\pi/2} \mathcal{D}_{\nu+2}^{\eta+2} \end{pmatrix}, \quad (6)$$

where $N_i = \sum_{\nu, \eta} |\mathcal{D}_{\nu}^{\eta}|^2$ is the normalization factor with $i = \{1, 2, 3, 4\}$ and $\mathcal{D} = \{\psi, \phi, \chi, \mu\}$.

Accordingly, pristine dipole elements $\mathcal{J}_{\alpha\beta,\nu\nu'}^{m'}(\vec{k})$ can also be calculated analytically,

$$\mathcal{J}_{xx;-1,+1}^{-1,-1}(\vec{k}) = \frac{e^2}{N_1 N_3} \left[2\zeta_{1/2}k_x (\psi_{+1}^{-1}\chi_{+1}^{-1} - \psi_{-1}^{-1}\chi_{-1}^{-1}) - \alpha_{R,1/2} (\psi_{+1}^{-1}\chi_{+1}^{-1} - \psi_{-1}^{-1}\chi_{-1}^{-1}) + \gamma (\psi_{+1}^{-1}\chi_{-1}^{-1} + \psi_{-1}^{-1}\chi_{+1}^{-1} - \psi_{-1}^{-1} - \chi_{-1}^{-1}) \right], \quad (7a)$$

$$\mathcal{J}_{xx;-1,+1}^{-1,+1}(\vec{k}) = \mathcal{J}_{xx;-1,+1}^{-1,-1}(\vec{k})|_{N_3 \mapsto N_4 \text{ and } \chi \mapsto \mu}, \quad (7b)$$

$$\mathcal{J}_{xx;-1,+1}^{+1,-1}(\vec{k}) = \mathcal{J}_{xx;-1,+1}^{-1,-1}(\vec{k})|_{N_1 \mapsto N_2 \text{ and } \chi \mapsto \phi}, \quad (7c)$$

$$\mathcal{J}_{xx;-1,+1}^{+1,+1}(\vec{k}) = \mathcal{J}_{xx;-1,+1}^{-1,-1}(\vec{k})|_{N_1 \mapsto N_2, N_3 \mapsto N_4 \text{ and } \psi \mapsto \phi, \chi \mapsto \mu}. \quad (7d)$$

with the following set of components:

$$\psi_{-1}^{-1} = \frac{-\alpha_{R,1/2}k - \tilde{\varepsilon} + \tilde{\zeta}k^2 - \mathcal{G}_{-1}(\vec{k})}{2\gamma k_+}, \quad (8a)$$

$$\psi_{+1}^{-1} = \frac{-\alpha_{R,1/2}k - \tilde{\varepsilon} - \tilde{\zeta}k^2 - \mathcal{G}_{-1}(\vec{k})}{2\gamma k}, \quad (8b)$$

$$\phi_{-1}^{-1} = \frac{-\alpha_{R,1/2}k - \tilde{\varepsilon} + \tilde{\zeta}k^2 + \mathcal{G}_{-1}(\vec{k})}{2\gamma k_+}, \quad (8c)$$

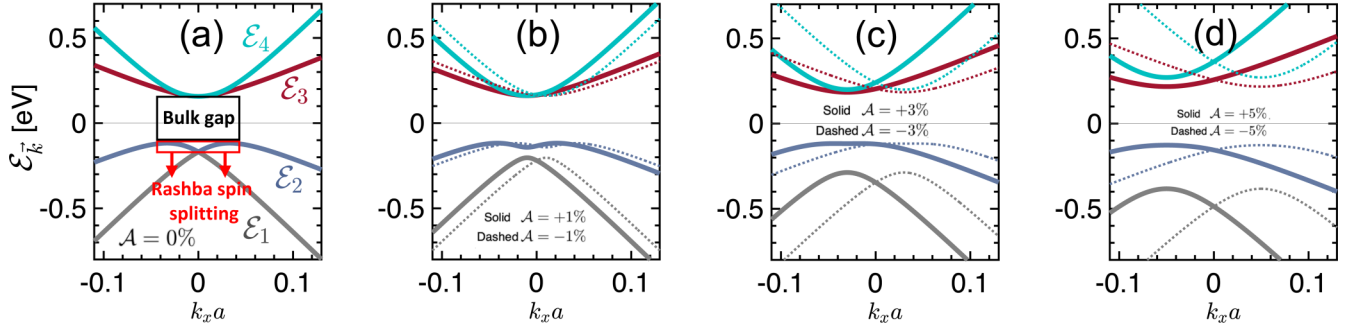


FIG. 2. Electronic band structure of monolayer PbBi along the x -direction at uniform strains including bulk gap and Rashba spin splitting gap: (a) $\mathcal{A}_x = \mathcal{A}_y = 0$, (b) $\mathcal{A}_x = \mathcal{A}_y = 1\%$, (c) $\mathcal{A}_x = \mathcal{A}_y = 3\%$, and (d) $\mathcal{A}_x = \mathcal{A}_y = 5\%$. Dashed lines indicate the same results for $\mathcal{A} < 0$. For uniform strains, all directions lead to the same bands.

$$\phi_{+1}^{-1} = \frac{-\alpha_{R,1/2}k - \tilde{\epsilon} - \tilde{\zeta}k^2 + \mathcal{G}_{-1}(\vec{k})}{2\gamma k}, \quad (8d)$$

$$\chi_{-1}^{-1} = \frac{+\alpha_{R,1/2}k - \tilde{\epsilon} + \tilde{\zeta}k^2 - \mathcal{G}_{+1}(\vec{k})}{2\gamma k_+}, \quad (8e)$$

$$\chi_{+1}^{-1} = \frac{+\alpha_{R,1/2}k - \tilde{\epsilon} - \tilde{\zeta}k^2 - \mathcal{G}_{+1}(\vec{k})}{2\gamma k}, \quad (8f)$$

$$\mu_{-1}^{-1} = \frac{+\alpha_{R,1/2}k - \tilde{\epsilon} + \tilde{\zeta}k^2 + \mathcal{G}_{+1}(\vec{k})}{2\gamma k_+}, \quad (8g)$$

$$\mu_{+1}^{-1} = \frac{+\alpha_{R,1/2}k - \tilde{\epsilon} - \tilde{\zeta}k^2 + \mathcal{G}_{+1}(\vec{k})}{2\gamma k}, \quad (8h)$$

where $\mathcal{G}_i(\vec{k})$ can be calculated from Eq. (3b). For all eigenstates, we have $\{\psi, \phi, \chi, \mu\}_{\pm 1}^{\pm 1} = 1$ and $\{\psi, \phi, \chi, \mu\}_{\pm 1}^{\pm 1} = k_-/k$.

Substituting $x \mapsto y$ and $k_x \mapsto k_y$, the equations along the y -direction can be obtained in the absence of strain. For the Hall component, multiplication of eigenstates along different directions is necessary, which is lengthy (not shown here).

Now, we proceed with the Kubo formula,⁵⁶ in which the optical conductivity tensor is given by

$$\sigma_{\alpha\beta}(\omega) = i \sum_{\vec{k}} \sum_{\nu\nu'\eta\eta'} \frac{f_{\vec{k},\nu}^{\eta} - f_{\vec{k},\nu'}^{\eta'}}{\mathcal{E}_{\vec{k},\nu}^{\eta} - \mathcal{E}_{\vec{k},\nu'}^{\eta'}} \frac{\mathcal{J}_{\alpha\beta;\nu\nu'}^{\eta\eta'}(\vec{k})}{\hbar\omega + i\delta + \mathcal{E}_{\vec{k},\nu}^{\eta} - \mathcal{E}_{\vec{k},\nu'}^{\eta'}}, \quad (9)$$

where $\delta = 3$ meV is a phenomenological factor and $f_{\vec{k},\nu/\nu'}$ is the Fermi-Dirac distribution function at $k_B T \simeq 50$ meV (k_B being the Boltzmann constant). In the presence of strain, the momenta in the eigenenergies are simply shifted by \vec{A} .

Although Eq. (9) gives rise to both intraband and interband optical transitions, we choose to only look at the interband ones. The reason for this can be justified by the fact that the intraband

part stems mainly from the scattering mechanisms with disorders, etc., whereas we do not have any scattering source in our model. Furthermore, we only focus on the real part of the optical conductivity tensor since the Kramers-Kronig relations⁵⁷ simply provide the imaginary part.

IV. RESULTS

In the following, we show the results of electronic band structure and optical conductivity in the presence of compressive and tensile strains. Also, we consider two classes of uniform and non-uniform strains. For the uniform strain, we have the same strengths along both x and y directions, i.e., $\mathcal{A} = \mathcal{A}_x = \mathcal{A}_y$, while for the non-uniform strain, we have different strengths along the x and y directions, i.e., $\mathcal{A}_x < \mathcal{A}_y$ or $\mathcal{A}_x > \mathcal{A}_y$.

We use the definitions $\mathcal{E}_1 = \mathcal{E}_{\vec{k},-1}^{-1}$, $\mathcal{E}_2 = \mathcal{E}_{\vec{k},-1}^{+1}$, $\mathcal{E}_3 = \mathcal{E}_{\vec{k},+1}^{-1}$, and $\mathcal{E}_4 = \mathcal{E}_{\vec{k},+1}^{+1}$ in Eq. (3) to understand the optical interband transitions. We set $\hbar = k_B = e = 1$ in the model so that we have optical responses in arbitrary units.

A. Uniform strain

In the absence of strain, the electronic band structure of monolayer PbBi is isotropic along the x and y directions^{44,51,58,59} and for this reason, we only show the x -direction. As expected, it contains four bands characterized by the bulk gap of 0.275 eV between the highest valence and lowest conduction bands, i.e., between \mathcal{E}_2 and \mathcal{E}_3 in Fig. 2(a), and by the Rashba-like spin splitting gap of 0.051 eV in the valence band between \mathcal{E}_1 and \mathcal{E}_2 . As a benchmark, we repeat the pristine band structure in Fig. 4(a).

In the presence of uniform strain, independent of the regime and class of strain, the immediate result is the disappearance of the Rashba spin splitting gap in the valence band, while the bulk gap is slightly changed compared to the Rashba spin splitting gap. This is in contrast to the consequence of other sources, e.g., it has been shown that an inversion symmetry breaking field can significantly tune the bulk gap,⁵⁹ but our findings show that it is robust against strain. Another point refers to the conduction band in which two bands do not touch each other anymore with strong strains. With tensile strains ($\mathcal{A} > 0$), the bands shift to the negative momenta,

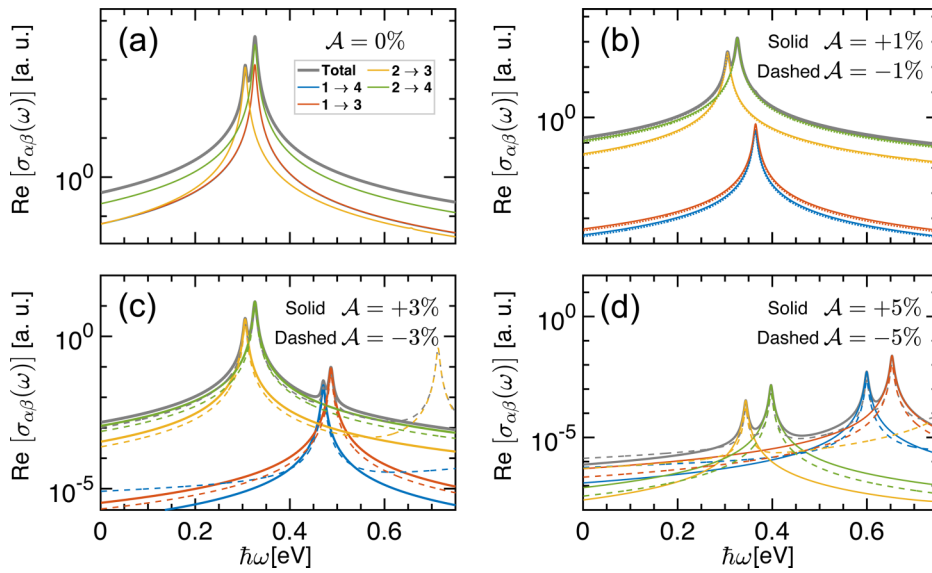


FIG. 3. Optical conductivity tensor of monolayer PbBiI in the presence of uniform strains: (a) $\mathcal{A}_x = \mathcal{A}_y = 0$, (b) $\mathcal{A}_x = \mathcal{A}_y = 1\%$, (c) $\mathcal{A}_x = \mathcal{A}_y = 3\%$, and (d) $\mathcal{A}_x = \mathcal{A}_y = 5\%$. Dashed lines indicate the same optical responses for $\mathcal{A} < 0$.

while they shift to the positive momenta with compressive strains ($\mathcal{A} < 0$) within the same manner. This confirms the following inversion symmetry in the structure once the strain is applied:

$$\mathcal{E}_{\vec{k}}(\vec{\mathcal{A}}) = -\mathcal{E}_{\vec{k}}(-\vec{\mathcal{A}}). \quad (10)$$

All these changes made by strain affect the optical interband transitions since Eq. (9) is tightly connected to the eigenstates and eigenvalues of the Hamiltonian. In the next analysis, we turn to the optical conductivity tensor. To address the interband transitions, we proceed with $\mathcal{E}_1 \rightarrow \mathcal{E}_3$, $\mathcal{E}_1 \rightarrow \mathcal{E}_4$, $\mathcal{E}_2 \rightarrow \mathcal{E}_3$, and $\mathcal{E}_2 \rightarrow \mathcal{E}_4$ in Fig. 1(a). In this setting, from the electronic band structure, the two first jumps are the same, while the two latter jumps are different due to the Rashba spin splitting gap. In the absence of strain, Fig. 3(a) and Ref. 59 first confirm the contribution of $\mathcal{E}_1 \rightarrow \mathcal{E}_3 = \mathcal{E}_1 \rightarrow \mathcal{E}_4$. This can be understood from Eqs. (7a) and (7d) such that terms in Eq. (8) lead to the same contributions of dipole elements. Second, two peaks appear in the optical conductivity; the first peak comes from $\mathcal{E}_2 \rightarrow \mathcal{E}_3$, while the second

peak originates from three other transitions. However, the dominant contribution belongs to $\mathcal{E}_2 \rightarrow \mathcal{E}_4$.

In the presence of 1% strain (almost independent of the type), we have three peaks in Fig. 3(b), but the third new peak is very small at a phonon energy of 0.37 eV. Two original peaks still correspond to $\mathcal{E}_2 \rightarrow \mathcal{E}_3$ and $\mathcal{E}_2 \rightarrow \mathcal{E}_4$, while the third one comes from the same contribution of $\mathcal{E}_1 \rightarrow \mathcal{E}_3$ and $\mathcal{E}_1 \rightarrow \mathcal{E}_4$, which are not the same anymore. Turning to the 3% strain in Fig. 3(c), one finds two and three extra peaks with compressive and tensile strain, respectively. Two extra optical peaks in the case of compressive 2% strain come from the different contribution of $\mathcal{E}_1 \rightarrow \mathcal{E}_3$ and $\mathcal{E}_1 \rightarrow \mathcal{E}_4$. However, three extra peaks in the case of tensile 3% strain appear due to transitions $\mathcal{E}_1 \rightarrow \mathcal{E}_3$, $\mathcal{E}_1 \rightarrow \mathcal{E}_4$, and $\mathcal{E}_2 \rightarrow \mathcal{E}_3$. Interestingly, for the same range of photon energy, a stronger 5% strain in Fig. 3(d) does only lead to two extra peaks from $\mathcal{E}_1 \rightarrow \mathcal{E}_3$ and $\mathcal{E}_1 \rightarrow \mathcal{E}_4$.

Overall, the appearance of extra peaks above two pristine peaks demonstrates that the system experiences a blueshift spectrum with uniform strain independent of direction. With blueshift, we mean that the strained lattice shows optical peaks at higher photon energies compared to the unstrained one such that the optical activity of the system is blueshifted with strain.

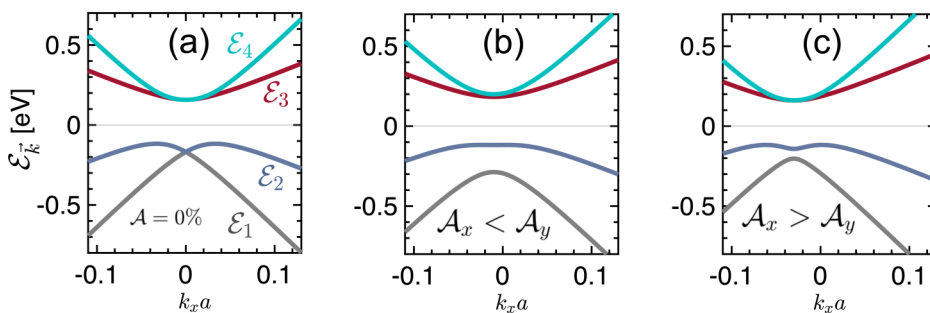


FIG. 4. Electronic band structure of monolayer PbBiI along the x-direction at non-uniform strains: (a) $\mathcal{A}_x = \mathcal{A}_y = 0$, (b) $(\mathcal{A}_x = 1\%) < (\mathcal{A}_y = 3\%)$, and (c) $(\mathcal{A}_x = 3\%) > (\mathcal{A}_y = 1\%)$. The symmetry $\mathcal{E}_{(k_x,0)}(\mathcal{A}_x < \mathcal{A}_y) = \mathcal{E}_{(0,k_y)}(\mathcal{A}_x > \mathcal{A}_y)$ is valid for non-uniform strains.

03 August 2023 13:08:43

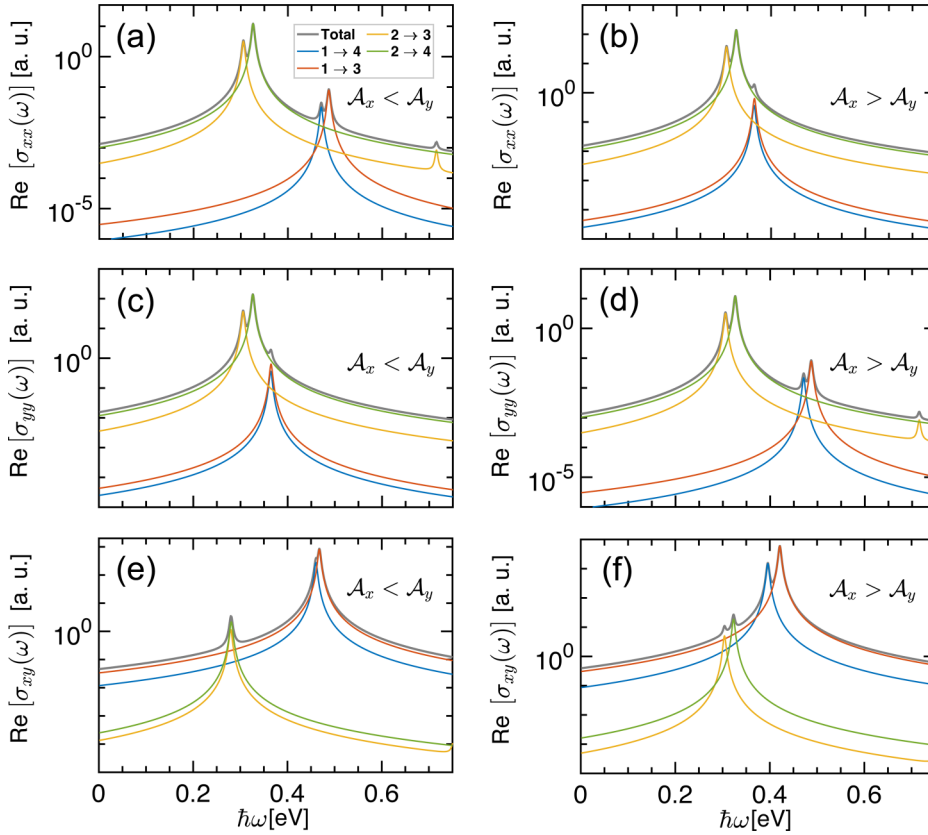


FIG. 5. [(a),(b)] and [(c),(d)] Optical conductivity of monolayer PbBiI along the x (y)-direction at non-uniform strains: [(a) and (c)] ($\mathcal{A}_x = 1\%$) $<$ ($\mathcal{A}_y = 3\%$) and [(b) and (d)] ($\mathcal{A}_x = 3\%$) $>$ ($\mathcal{A}_y = 1\%$). The symmetries $\sigma_{xx}(\mathcal{A}_x < \mathcal{A}_y) = \sigma_{yy}(\mathcal{A}_x > \mathcal{A}_y)$ and $\sigma_{yy}(\mathcal{A}_x < \mathcal{A}_y) = \sigma_{xx}(\mathcal{A}_x > \mathcal{A}_y)$ are evident. [(e) and (f)] Hall optical conductivity of monolayer PbBiI at non-uniform strains: (e) ($\mathcal{A}_x = 1\%$) $<$ ($\mathcal{A}_y = 3\%$) and (f) ($\mathcal{A}_x = 3\%$) $>$ ($\mathcal{A}_y = 1\%$).

B. Non-uniform strain

In contrast to the uniform class of strain, we do not consider simultaneous compressive and tensile strains when comparing the strains along the x and y directions. Starting with the band structure in Fig. 4, one can see that the Rashba spin splitting gap is disappeared with non-uniform strains $\mathcal{A}_x < \mathcal{A}_y$ much faster than $\mathcal{A}_x > \mathcal{A}_y$. Additionally, conduction bands only keep the contact for $\mathcal{A}_x > \mathcal{A}_y$. Although we have not shown the corresponding band structure, from the inversion symmetry of the Rashba term, it is not hard to conclude

$$\mathcal{E}_{(k_x,0)}(\mathcal{A}_x < \mathcal{A}_y) = \mathcal{E}_{(0,k_y)}(\mathcal{A}_x > \mathcal{A}_y). \quad (11)$$

We confirm this in the optical conductivity data in the following.

In Fig. 5(a), we show that the non-uniform strain $\mathcal{A}_x < \mathcal{A}_y$ adds three extra optical peaks at higher photon energies to the pristine ones along the x -direction. Our analysis reports the contribution of $\mathcal{E}_1 \rightarrow \mathcal{E}_4$, $\mathcal{E}_1 \rightarrow \mathcal{E}_3$, and $\mathcal{E}_2 \rightarrow \mathcal{E}_3$ optical transitions for these peaks, respectively. On the other hand, for $\mathcal{A}_x > \mathcal{A}_y$, one finds a small extra peak mainly from $\mathcal{E}_1 \rightarrow \mathcal{E}_4$ and $\mathcal{E}_1 \rightarrow \mathcal{E}_3$, as shown in Fig. 5(b). This, in turn, confirms the central role of $\mathcal{A}_x < \mathcal{A}_y$ in eliminating the Rashba spin splitting gap. Moreover,

following Eq. (11), we simply expect

$$\begin{aligned} \sigma_{xx}(\mathcal{A}_x < \mathcal{A}_y) &= \sigma_{yy}(\mathcal{A}_x > \mathcal{A}_y) \quad \text{and} \\ \sigma_{xx}(\mathcal{A}_x > \mathcal{A}_y) &= \sigma_{yy}(\mathcal{A}_x < \mathcal{A}_y). \end{aligned} \quad (12)$$

This is confirmed in Figs. 5(c) and 5(d). So, the above analysis only needs to be swapped for the optical conductivity along the y -direction. As for the basic physics behind such anisotropy, we see that a non-uniform class of strain modifies hopping energies differently along different directions and this, in turn, leads to an anisotropic optical conductivity as the Kubo formula mainly works with eigenstates and eigenenergies.

Finally, in Figs. 5(e) and 5(f), we address how strain affects the Hall optical conductivity of monolayer PbBiI. For $\mathcal{A}_x < \mathcal{A}_y$ non-uniform strains, although we still have two optical peaks, their positions are shifted with strain. We find that the first peak corresponds to the transitions $\mathcal{E}_2^x \rightarrow \mathcal{E}_3^y$ and $\mathcal{E}_2^x \rightarrow \mathcal{E}_4^y$, while the second peak originates from $\mathcal{E}_1^x \rightarrow \mathcal{E}_3^y$ and $\mathcal{E}_1^x \rightarrow \mathcal{E}_4^y$. However, for $\mathcal{A}_x > \mathcal{A}_y$ strains, we have two extra optical peaks in addition to the original pristine ones and $\mathcal{E}_1^x \rightarrow \mathcal{E}_3^y$ and $\mathcal{E}_1^x \rightarrow \mathcal{E}_4^y$ are responsible for these extra transitions. In contrast to the uniform strains, such a structure for optical peaks reports that the system intends to be anisotropic with non-uniform ones. Furthermore, we still have a blueshift spectrum with non-uniform strains.

V. SUMMARY

PbBiI monolayer is notable for its Rashba spin-orbit coupling and unconventional spin texture. Using the Kubo formula, Peierls substitution, and Kane-Mele model in the presence of strain, we have shown that strain can destroy the Rashba spin splitting gap, while the bulk gap is not strongly affected. Consequently, optical conductivity presents a blueshift spectrum independent of the class and type of strain. Interestingly, our calculations for non-uniform strains result in anisotropic interband optical transitions. Overall, these findings propose a path for tuning the electro-optical features of PbBiI in real applications.

ACKNOWLEDGMENTS

This work was supported by Hue University under the Core Research Program, Grant No. NCM.DHH.2020.01.

AUTHOR DECLARATIONS

Conflict of Interest

The authors have no conflicts to disclose.

Author Contributions

Bui D. Hoi: Conceptualization (equal); Data curation (equal); Formal analysis (equal); Funding acquisition (equal); Investigation (equal); Methodology (equal); Resources (equal); Software (equal); Validation (equal); Visualization (equal); Writing – original draft (equal); Writing – review & editing (equal).

DATA AVAILABILITY

The data that support the findings of this study are available from the corresponding author upon reasonable request.

REFERENCES

- ¹K. S. Novoselov, D. Jiang, F. Schedin, T. J. Booth, V. V. Khotkevich, S. V. Morozov, and A. K. Geim, *Proc. Natl. Acad. Sci.* **102**, 10451 (2005).
- ²K. S. Novoselov, A. K. Geim, S. V. Morozov, D. Jiang, Y. Zhang, S. V. Dubonos, I. V. Grigorieva, and A. A. Firsov, *Science* **306**, 666 (2004).
- ³K. S. Novoselov, *Rev. Mod. Phys.* **83**, 837 (2011).
- ⁴M. Z. Hasan and C. L. Kane, *Rev. Mod. Phys.* **82**, 3045 (2010).
- ⁵B. Yan and S.-C. Zhang, *Rep. Prog. Phys.* **75**, 096501 (2012).
- ⁶C. L. Kane and E. J. Mele, *Phys. Rev. Lett.* **95**, 226801 (2005).
- ⁷B. A. Bernevig, T. L. Hughes, and S.-C. Zhang, *Science* **314**, 1757 (2006).
- ⁸M. König, S. Wiedmann, C. Brüne, A. Roth, H. Buhmann, L. W. Molenkamp, X.-L. Qi, and S.-C. Zhang, *Science* **318**, 766 (2007).
- ⁹L. Kou, Y. Ma, Z. Sun, T. Heine, and C. Chen, *J. Phys. Chem. Lett.* **8**, 1905 (2017).
- ¹⁰M. Yarmohammadi, M. Bukov, and M. H. Kolodrubetz, *Phys. Rev. B* **107**, 054439 (2023).
- ¹¹J. Nitta, T. Akazaki, H. Takayanagi, and T. Enoki, *Phys. Rev. Lett.* **78**, 1335 (1997).
- ¹²T. Hirahara, T. Nagao, I. Matsuda, G. Bihlmayer, E. V. Chulkov, Y. M. Koroteev, P. M. Echenique, M. Saito, and S. Hasegawa, *Phys. Rev. Lett.* **97**, 146803 (2006).
- ¹³S. Mathias, A. Ruffing, F. Deicke, M. Wiesenmayer, I. Sakar, G. Bihlmayer, E. V. Chulkov, Y. M. Koroteev, P. M. Echenique, M. Bauer, and M. Aeschlimann, *Phys. Rev. Lett.* **104**, 066802 (2010).

- ¹⁴H. Yuan, M. S. Bahramy, K. Morimoto, S. Wu, K. Nomura, B.-J. Yang, H. Shimotani, R. Suzuki, M. Toh, C. Kloc, X. Xu, R. Arita, N. Nagaosa, and Y. Iwasa, *Nat. Phys.* **9**, 563 (2013).
- ¹⁵J. H. Dil, F. Meier, J. Lobo-Checa, L. Patthey, G. Bihlmayer, and J. Osterwalder, *Phys. Rev. Lett.* **101**, 266802 (2008).
- ¹⁶X.-L. Qi and S.-C. Zhang, *Rev. Mod. Phys.* **83**, 1057 (2011).
- ¹⁷S. Maekawa, S. Valenzuela, E. Saitoh, and T. Kimura, *Spin Current*, Series on Semiconductor Science and Technology (OUP Oxford, 2012).
- ¹⁸A. Manchon, H. C. Koo, J. Nitta, S. M. Frolov, and R. A. Duine, *Nat. Mater.* **14**, 871 (2015).
- ¹⁹D. Bercioux and P. Lucignano, *Rep. Prog. Phys.* **78**, 106001 (2015).
- ²⁰A. Ström, H. Johannesson, and G. I. Japaridze, *Phys. Rev. Lett.* **104**, 256804 (2010).
- ²¹J. C. Budich, F. Dolcini, P. Recher, and B. Trauzettel, *Phys. Rev. Lett.* **108**, 086602 (2012).
- ²²F. M. C. Crépin, J. C. Budich, F. Dolcini, P. Recher, and B. Trauzettel, *Phys. Rev. B* **86**, 121106 (2012).
- ²³T. L. Schmidt, S. Rachel, F. von Oppen, and L. I. Glazman, *Phys. Rev. Lett.* **108**, 156402 (2012).
- ²⁴J. I. Väyrynen, M. Goldstein, and L. I. Glazman, *Phys. Rev. Lett.* **110**, 216402 (2013).
- ²⁵F. Geissler, F. M. C. Crépin, and B. Trauzettel, *Phys. Rev. B* **89**, 235136 (2014).
- ²⁶K. Jiang, S. Zhou, X. Dai, and Z. Wang, *Phys. Rev. Lett.* **120**, 157205 (2018).
- ²⁷M. König, H. Buhmann, L. W. Molenkamp, T. Hughes, C.-X. Liu, X.-L. Qi, and S.-C. Zhang, *J. Phys. Soc. Jpn.* **77**, 031007 (2008).
- ²⁸B. Scharf, A. Matos-Abiague, and J. Fabian, *Phys. Rev. B* **86**, 075418 (2012).
- ²⁹P. Debray, S. M. S. Rahman, J. Wan, R. S. Newrock, M. Cahay, A. T. Ngo, S. E. Ulloa, S. T. Herbert, M. Muhammad, and M. Johnson, *Nat. Nanotechnol.* **4**, 759 (2009).
- ³⁰P. Chuang, S.-C. Ho, L. W. Smith, F. Sfigakis, M. Pepper, C.-H. Chen, J.-C. Fan, J. P. Griffiths, I. Farrer, H. E. Beere, G. A. C. Jones, D. A. Ritchie, and T.-M. Chen, *Nat. Nanotechnol.* **10**, 35 (2015).
- ³¹A. T. Ngo, P. Debray, and S. E. Ulloa, *Phys. Rev. B* **81**, 115328 (2010).
- ³²M. Yarmohammadi, B. D. Hoi, and L. T. T. Phuong, *Sci. Rep.* **11**, 3716 (2021).
- ³³M. Yarmohammadi, M. M. Nobahari, T. S. Tien, and L. T. T. Phuong, *J. Phys.: Condens. Matter.* **32**, 465301 (2020).
- ³⁴B. D. Hoi, M. Yarmohammadi, and H. A. Kazzaz, *J. Magn. Magn. Mater.* **439**, 203 (2017).
- ³⁵W. Sun, X. Li, B. Li, X. Zou, B. Huang, Y. Dai, and C. Niu, *J. Phys. D: Appl. Phys.* **55**, 305301 (2022).
- ³⁶H. Zhang, Y. Ma, and Z. Chen, *Nanoscale* **7**, 19152 (2015).
- ³⁷Y. Ma, Y. Dai, W. Wei, B. Huang, and M.-H. Whangbo, *Sci. Rep.* **4**, 7297 (2014).
- ³⁸C. Huang, J. Zhou, H. Wu, K. Deng, P. Jena, and E. Kan, *Phys. Rev. B* **95**, 045113 (2017).
- ³⁹H. Shi, H. Pan, Y.-W. Zhang, and B. I. Yakobson, *Phys. Rev. B* **87**, 155304 (2013).
- ⁴⁰Z. Peng, X. Chen, Y. Fan, D. J. Srolovitz, and D. Lei, *Light: Sci. Appl.* **9**, 190 (2020).
- ⁴¹J. Du, H. Yu, B. Liu, M. Hong, Q. Liao, Z. Zhang, and Y. Zhang, *Small Methods* **5**, 2000919 (2021).
- ⁴²K. Beach, M. C. Lucking, and H. Terrones, *Phys. Rev. B* **101**, 155431 (2020).
- ⁴³S. Yang, Y. Chen, and C. Jiang, *InfoMat* **3**, 397 (2021).
- ⁴⁴C. Mera Acosta, O. Babilonia, L. Abdalla, and A. Fazzio, *Phys. Rev. B* **94**, 041302 (2016).
- ⁴⁵N. A. Gokcen, *J. Phase Equilib.* **13**, 21 (1992).
- ⁴⁶H. W. Huang and C. M. Serrano, *J. Vac. Sci. Technol. A* **1**, 1409 (1983).
- ⁴⁷T. K. Drozdov, A. Alexandradinata, S. Jeon, S. Nadj-Perge, H. Ji, R. J. Cava, B. Andrei Bernevig, and A. Yazdani, *Nat. Phys.* **10**, 664 (2014).
- ⁴⁸R. Yu, X. L. Qi, A. Bernevig, Z. Fang, and X. Dai, *Phys. Rev. B* **84**, 075119 (2011).
- ⁴⁹A. A. Soluyanov and D. Vanderbilt, *Phys. Rev. B* **83**, 035108 (2011).

- ⁵⁰A. A. Soluyanov and D. Vanderbilt, *Phys. Rev. B* **83**, 235401 (2011).
- ⁵¹L. T. T. Phuong, T. C. Phong, B. D. Hoi, and M. Yarmohammadi, *J. Mater. Chem. A* **10**, 16620 (2022).
- ⁵²S. Fang, S. Carr, M. A. Cazalilla, and E. Kaxiras, *Phys. Rev. B* **98**, 075106 (2018).
- ⁵³M. Yarmohammadi, *AIP Adv.* **6**, 085008 (2016).
- ⁵⁴M. Yarmohammadi and M. R. Ebrahimi, *Phys. Rev. B* **100**, 165409 (2019).
- ⁵⁵L. T. T. Phuong, T. C. Phong, and M. Yarmohammadi, *Sci. Rep.* **10**, 9201 (2020).
- ⁵⁶G. Mahan, *Many-Particle Physics*, Physics of Solids and Liquids (Springer US, 2000).
- ⁵⁷R. D. L. Kronig and H. A. Kramers, *Z. Phys.* **48**, 174 (1928).
- ⁵⁸T. Phong, V. T. Lam, and B. D. Hoi, *J. Phys.: Condens. Matter.* **33**, 325502 (2021).
- ⁵⁹B. D. Hoi, *Phys. Rev. B* **106**, 165424 (2022).